RESEARCH PAPER

Enhanced Photocatalytic Activity with Sulphur-rich CuS Nanoparticles Grown by Hydrothermal Route

UPS. Gahlaut, Y.C. Goswami*, Jyoti Bala

* *ycgoswami@gmail.com*

Nano Research Lab, Department of Physics, SOS, ITM University Gwalior, MP 474001, India

Received: July 2024 **Revised: June 2025** **Accepted: July 2025**
DOI: 10.22068/ijmse.3671

Abstract: *Highly active CuS nanoparticles (NPs) were synthesized using a hydrothermal route with various sulphur ratios. The comprehensive characterization of these NPs involved an analysis of their structure, composition, and optical properties, primarily conducted through X-ray diffraction (XRD) analysis. The XRD pattern confirmed the presence of the hexagonal phase in the CuS particles. The investigation further determined an estimated bandgap energy of 3.80 eV for the slightly sulphur-rich CuS NPs. Notably, this energy value exceeds that of bulk CuS, indicating a noticeable miniaturization effect. The novel CuS NPs exhibited outstanding photocatalytic activity in the degradation of methyl Red (MR), particularly under visible light. This impressive performance is attributed to surface-bound OH ions on the CuS nanostructures, facilitating the adsorption and acceleration of the degradation process for MR molecules under visible light irradiation. The research highlights the significant promise and efficiency of the synthesized CuS NPs as photocatalysts. These nanoparticles are exceptionally responsive to stable visible light, making them highly suitable for purifying chemically contaminated wastewater. Specifically, their effectiveness in degrading stable azo dyes, exemplified by MR, underscores their potential in practical applications.*

Keywords: *Photocatalysts, CuS, Hexagonal, Optical properties, Hydrothermal, Nanostructures.*

1. INTRODUCTION

Semiconductor nanomaterials exhibit distinct properties compared to their bulk counterparts, driven by factors such as their surface-to-volume ratio and confinement of electrons within three dimensions [1-4]. These unique attributes have sparked considerable interest in their exploration. Transition metal chalcogenides, due to their novel physical and chemical characteristics, have recently garnered substantial attention. Metal sulphides, as a significant class of semiconductors, offer tunable band gaps via control over particle size. Among these sulfides, CuS stands out as an exceptional semiconducting material with vast potential across domains. Copper sulphide is a p-type semi-conductor that possesses a crystalline phase-dependent band gap spanning 1.48 eV to 2.89 eV [5]. This range notably aligns with the energy spectrum of ultraviolet and visible light [6]. Like solar cells, photocatalysis, supercapacitors, photothermal conversion, and surface plasmon resonance absorption. This intriguing alignment underscores CuS strong capacity for absorbing ultraviolet and visible light suitable for applications like photocatalytic pollutant degradation [7]. The placement of HOMO (Highest occupied Molecular Orbit) and LUMO (Least Occupied Molecular orbit) of CuS on energy scale at 5.1 ev and 2.9 ev respectively enables CuS nanostructures applications in solar cells [8-9]. High energy Capacity (560 mA $h^{-1}g$) and good electronic conductivity (10^3 $S^{-1}cm$) enable CuS to be applied as a suitable material for the cathode in lithium batteries [9-10]. A recent research article has also reported the use of CuS as a glucose and DNA sensor [11]. Due to their better physicochemical and pharmacokinetic characteristics compared to gold, silver nanomaterials and copper sulphide nanostructures have attracted attention in the biomedical field. [11] CuS nanostructures can absorb from 400 to 550 nm due to their unique size-dependent properties and provide a strong blue emission band at 465 nm. This makes CuS an excellent photo luminescent material, which enables its use in biological labelling and light-emitting devices [9]. Recent research papers indicate that Cus nanorods can transmit 50% of visible light (300-650 nm). This transparency in the UV and near-IR region enables the use of CuS in spectrally selective window coatings [12]. The physicochemical attributes of CuS undergo significant alterations upon scaling down to the nanoscale, owing to the quantum size effect. Wang (2016) [13] reported the application of CuS nanoparticles in imaging and cancer therapy. Similar work was also reported for gold/hydroxyl-propyl cellulose hybrid nanocomposites and

Bi-Oxide nanoparticle ZnO/CuO [14, 15]. He et al. (2012) studied peroxidase-like activities using CuS and its superstructures [16].

Various synthesis methods have been reported for synthesise CuS nanostructures [17], including solvothermal (Cheng et al. 2010, 2013), thermolysis, sonochemical, and hydrothermal approaches [18-21]. Among these, the hydrothermal method has emerged as a prominent technique, primarily due to its versatility and reproducibility. The morphologies of CuS nanoparticles are strongly influenced by precursor concentration, surfactant presence, and reaction parameters, including temperature and duration [22-26]. Many Research groups have reported the photocatalytic activity of CuS nanoparticles on dyes such as MB (Methylene Blue), CR (Congo Red), and RhB (Rhodamine B) [27-29], with percentage degradation ranging from 50 to 94. In comparison to them, not only is our percentage degradation of 96 higher, but our preparation method is also fast, simple, ecological, and low-cost.

In the present work, we successfully synthesized intriguing copper sulphide nanostructures using a cost-effective and straightforward hydrothermal method, where ethylene glycol (EG) served as the surfactant, and water functioned as the solvent. The surfactant played a pivotal role in determining the morphology of CuS and conferring stability to the nanostructures [30]. The synthesis process employed copper chloride and thiourea as copper and sulphur sources, respectively, in the presence of EG surfactant at 150°C for four hours, with varying concentrations of thiourea. CuS, a p-type semiconductor, is known for its excellent photocatalytic degradation activity and superior absorption of solar radiation, making it an ideal candidate for dye removal applications [31-32].

2. EXPERIMENTAL PROCEDURES

2.1. Materials

Thiourea, Copper chloride, and Ethylene glycol (EG) were utilized as received, without the need for further purification. These chemicals were of analytical reagent (AR) grade and were procured from Sigma Aldrich. Distilled water, freshly prepared, was employed as the solvent during the synthesis.

2.2. Synthesis Steps

The synthesis comprised three distinct steps:

2.2.1. Preparation of solvent

A solvent was first prepared by blending 30 mL of distilled water with 70 mL of ethylene glycol (EG), with continuous stirring for 30 minutes. Following vigorous stirring, the resulting solution was divided into four equal portions.

2.2.2. Preparation of Copper sulphide solution

In the initial portion of the solvent, a mixture of 0.1 M CuCl and 0.1 M thiourea was dissolved in a beaker, which was then subjected to ultrasonication for 1 hour at 40°C. Subsequently, CuCl and thiourea were mixed in varying ratios of 1:1, 1:3, 1:5, and 1:7. These mixtures were then placed in an autoclave and maintained at 150°C for 4 hours. This process was replicated for each of the three ratios. After aging for three days, the resulting solutions were labelled S1, S2, S3, and S4, corresponding to the different ratios.

2.2.3. Photocatalytic experiment

Photocatalytic experiments were conducted employing ammonia-doped CuS nanostructures to catalyze the decomposition of a dye. A 10 ppm solution of methyl red was prepared, maintaining a pH of 6.

The absorbance maximum of methyl red was identified at 464 nm, serving as the reference wavelength for all absorbance measurements. In each of the four separate beakers, 20 mL of the methyl red solution was dispensed, followed by the addition of 0.2 g of photocatalyst powder. Subsequent stirring occurred in a dark environment before transferring the beakers to a self-constructed photocatalytic reactor equipped with a 36 watt white light source. The reaction rate was assessed utilizing Beer-Lambert's law (Eq. (1)), and the rate constant (k) was determined employing Eq. (2).

$$\text{Degaradtion\%} = \left(1 - \frac{A}{A_0}\right) \times 100 \quad (1)$$

Where A is the concentration of dye at time t and A_0 is the concentration at time t=0. for the rate constant, we used another equation

$$K = \log(A_0/A)/t \quad (2)$$

2.3. Characterization

X-Ray Diffraction (XRD) Analysis was carried out using a 300/650 Miniflex instrument. The analysis spanned a 2θ range from 20° to 80°. Fourier Transform Infrared (FTIR) Analysis. Functional analysis was conducted using a Perkin Elmer instrument. UV-Visible Absorption Studies. Absorption studies were performed

using a Perkin-Elmer Lambda–25 UV-Visible Spectroscopy instrument. Photoluminescence (PL) Studies Photoluminescence (PL) studies were carried out using a Perkin Elmer LS-55 instrument at PC Ray Centre, ITM University, Gwalior.

3. RESULTS AND DISCUSSION

3.1. Structural Characterization

The XRD spectra of the synthesized CuS nanostructures at different precursor ratios (a) 1:1 (b) 1:3 (c) 1:5 and (d) precursor ratio 1:7 shown in Fig. 1. Spectra indicate that all apparent peaks are assigned to the hexagonal crystal structure of CuS (JCPDS 78-0876), with no additional peaks. The XRD results indicate the high purity of the hydrothermally synthesized products. This result is in good agreement with previous reports showing multiphase CuS. All [33] diffraction peaks of the CuS crystal structure are identified.

The crystallite size (D) and microstrain (ε) of the resulting CuS nanocomposites can be calculated from the XRD patterns using Williamson Hall analysis [34] (graph in Fig. 2). The first is responsible for the crystallite size (D), and the second reflects the strain effect (ε):

$$\beta = \beta D + \beta\varepsilon \quad (3)$$

The Williamson-Hall equation can be written as follows:

$$\beta \cos\theta = k\frac{k}{D} + 4\varepsilon \sin\theta \quad (4)$$

The crystallite size of CuS nanocomposites is calculated using the Debye-Scherrer equation [35]. The calculated microstrain of the material is 0.77 nm for all samples, with a consistent fringe width. The particles exhibit approximately the same size, at 75.10 nm. And have a negative slope. All the samples exhibit almost identical data; there is no change in XRD data. The slope is negative, confirming the presence of compressive strain.

$$D = {}^{0.9\lambda}/_{\beta\cos\theta}$$

3.2. FTIR Studies

Fig. 3. IR spectroscopy shows that CuS and its complexes have properly prepared a peak residing at 3358 cm^{-1}.

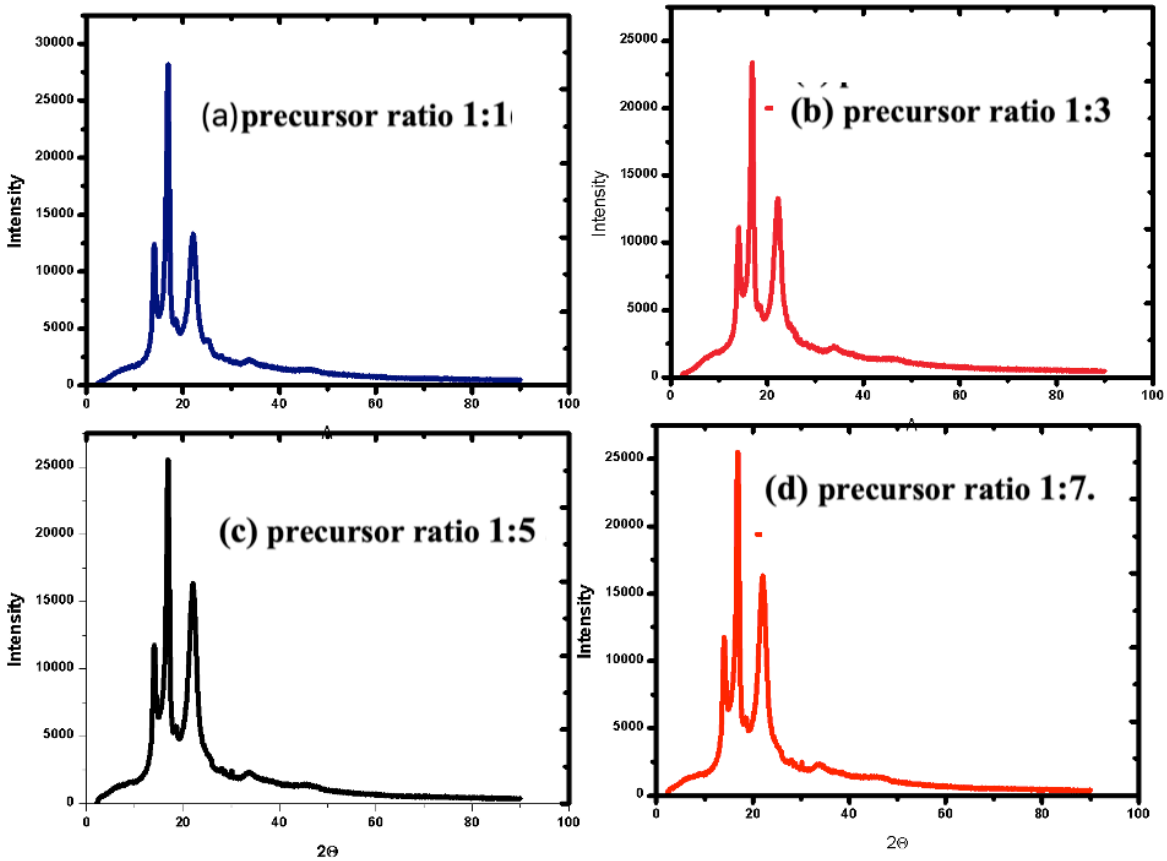

Fig. 1. X-Ray diffractograms of CuS nanocomposite a) precursor ratio 1:1, b) precursor ratio 1:3, c) precursor ratio 1:5, and d) precursor ratio 1:7

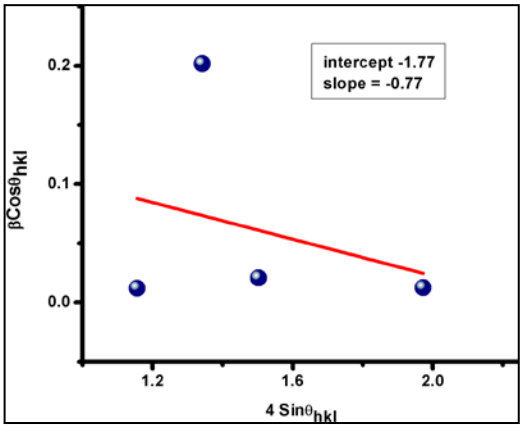

Fig. 2. W-H Plots of CuS nanocomposite

This corresponds to the stretching frequencies of epoxide C-O bonds and dangling -OH bonds [36]. The intensity of the peak increases with the addition of S nanoparticles to CuS. The peak at 1588 cm^{-1} is assigned to the extension frequency of carbonyl C=O bonds, and the peak at 1386 cm^{-1} indicates CH_2. The peak at 631 cm^{-1} indicates a stretching vibration. Table 1 shows all the peaks obtained from the IR data [37].

3.3. Optical Studies

The optical bandgap (Eg) of CuS at various proportions of S in CuS (a) precursor ratio 1:1 (b) precursor ratio 1:3 (c) precursor ratio 1:5 and (d) precursor ratio 1:7 was calculated with the help of Tauc relation and absorption spectra [38-40] shown in Fig. 4.

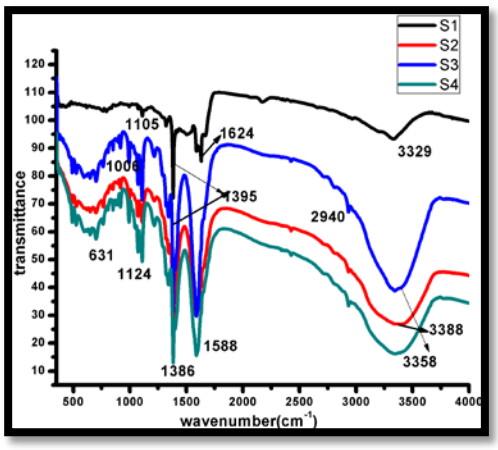

Fig. 3. FTIR-Spectrum Bands Wave numbers cm^{-1} attributed to stretching vibrations

$(\alpha h\upsilon)^2 = A((h\upsilon - E_g)$

Where $h\upsilon$ is the photon energy and α is the absorption coefficient. E_g is the optical bandgap. The values of the optical bandgap E_g of the CuS nanocomposite sample were determined to be (a) 3.80 eV, (b) 3.85 eV, (c) 3.83 eV, and (d) 3.7 eV.

Table 1. IR-Spectrum Bands Wave numbers cm^{-1} attributed stretching vibrations

Stretching	S1	S2	S3	S4
	Wavenumber cm^{-1}			
O-H stretching	3358	3388	3358	3329
C=C	1588	1588	1588	1624
C-C	1386	1395	1395	1395
C-H	1124	1124	1006	1105
Cu-S	631	631	631	631

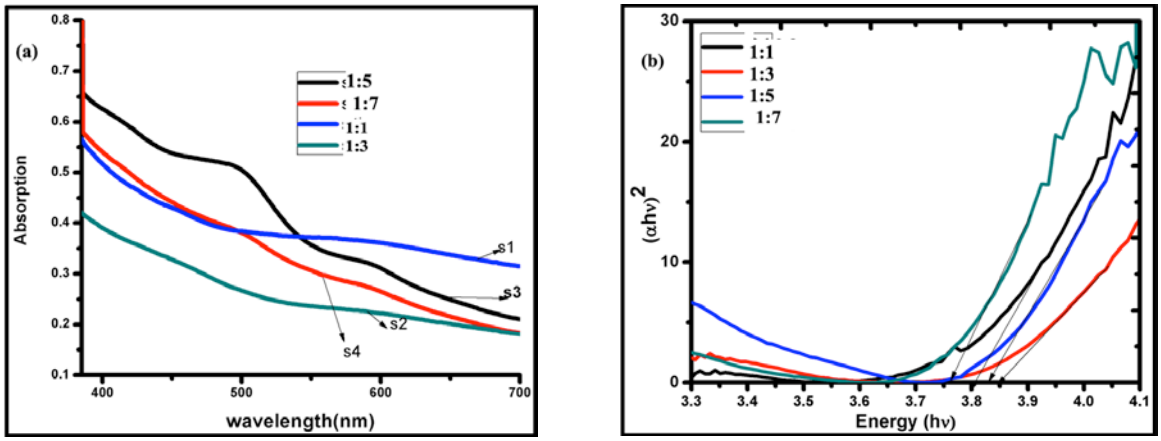

Fig. 4. a) Absorption spectra and b) tauc plot of CuS nanostructures grown with various precursor ratios 1:1, 1:3, 1:5 and 1:7

The optical bandgap of CuS nanocomposites decreases with increasing concentration of Sulphur in CuS. The decrease in the bandgap of CuS can be explained by the increased surface charge between Cu and S, resulting in a shift of the optical bandgap to longer wavelengths. The S2 and S3 samples have slightly larger band gaps than the S1 and S4 samples.

3.4. . Photo Luminescence Studies (PL)

Photoluminescence spectra for CuS samples were carried out and are shown in Fig. 5. Broad peaks at 350 nm and 450 nm for all samples S1, S2, S3, and S4 are observed. By increasing the sulphur content of Cu, the intensity is reduced, and the broadness of luminescence peaks decreases.

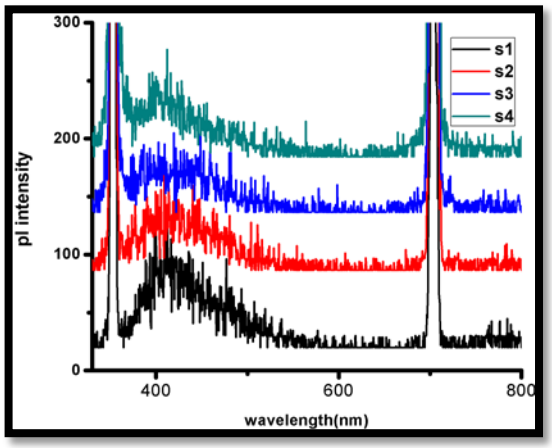

Fig. 5. Pl spectra of CuS nanocomposites

3.5. Photocatalytic Activity

As the samples are exposed to increasing light intensity and longer illumination times, a reduction in dye absorption becomes evident. This trend is illustrated graphically in Figure 6, showing a decline in dye concentration with increasing light irradiation. It is worth noting that the incorporation of Cu within the photocatalyst system plays a pivotal role in enhancing carrier separation and augmenting light absorption. Similar observations were reported [39-41].

3.5.1. Percentage degradation of dyes

The percentage of photocatalytic degradation was computed using equation (1). A graphical representation of the per cent degradation is presented in Fig. 7.

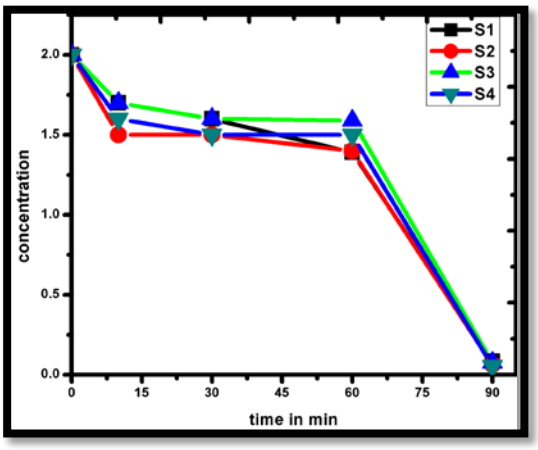

Fig. 6. Concentration vs. time graph of CuS nanocomposite for MR dye

As the sulphur (S) content in the Cu ratio decreases, the decomposition rate reaches a value of 93.9%. Conversely, the decomposition rate increases in tandem with the elevated S content within the Cu. Remarkably, the fourth sample, which harbours a substantial proportion of S nanoparticles in Cu, achieves an impressive 96.3% dye removal from the water in just 190 minutes. For comprehensive information on the calculated rate constants and degradation rate values, kindly refer to Table 2.

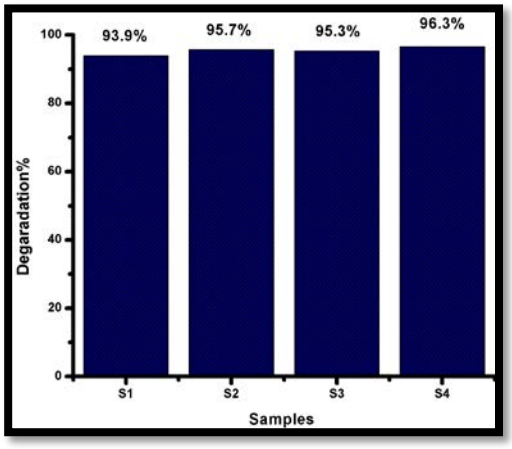

Fig. 7. Histogram of Percentage degradation in photocatalytic activity

Table 2. Rate constant and degradation value

Samples	S1	S2	S3	S4
Rate constant (K)	0.00393	0.004	0.00393	0.00403
Degradation %	93.9	95.7	95.3	96.3

3.5.2. *Mechanism of the chemical equation*

The photocatalytic activity was conducted using a 36 watt LED light setup for 190 minutes. In this assessment, the degradability of the catalyst was examined using methyl red dye. A depiction of the photocatalytic activity mechanism involving MR dye and CuS nanoparticles is presented in Figure 8. When the incident light encounters the catalyst, it initiates the generation of electrons and holes. The adsorption mechanism involves electrostatic repulsion between the dye and the CuS catalyst nanoparticles. Among the samples, S4 exhibited superior degradation performance.

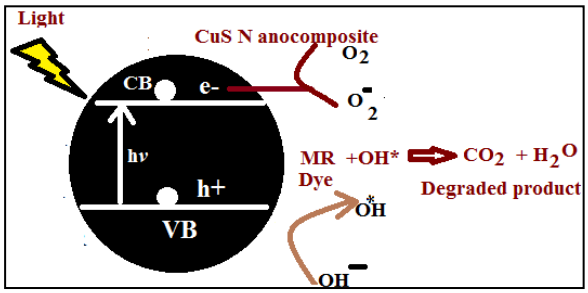

Fig. 8. Mechanism of photocatalytic activity of MR dye with CuS nanoparticles

Notably, since methyl red is an anionic dye, it interacts with the holes within the catalyst, leading to its decomposition [39-41]. Moreover, these holes react with hydroxyl ions, yielding additional OH* free radicals, which contribute to the degradation process. The concentration versus time graph assumes a linear profile, consistent with a first-order kinetic pseudo-reaction [41].

Under UV-visible light, photocatalytic activity occurs due to the absorption of photons, resulting in the movement of electrons and holes to the conduction and valence bands, respectively. The electrons on the surface of the conduction band of CuS react with oxygen molecules to generate superoxide ($O_2^{\bullet-}$) anion radicals [42], and the separated holes in the valence bands of CuS effectively oxidize H_2O into hydroxyl radicals ($OH^{\bullet}$) [43]. Consequently, the $OH^{\bullet}$ and $O_2^{\bullet-}$ radicals react with Methyl red dye and degrade it into nontoxic and inorganic products (e.g., H_2O and CO_2). The operating mechanism is illustrated in Figure 8.

$$CuS + h\nu \xrightarrow{CuS} (e^- + h^+)$$
$$O_2 + e^- \rightarrow O_2^-$$
$$O_2^- + H_2O \rightarrow H_2O_2$$
$$H_2O_2 \rightarrow 2OH^*$$
$$H_2O + h^+ \rightarrow OH^* + H^+$$
$$OH^* + \text{methyl Red Dye} \rightarrow \text{degraded product}$$

4. CONCLUSIONS

In this study, we successfully synthesised CuS nanoparticles (NPs) with nanometer-scale dimensions utilizing a wet chemical method. The XRD pattern unequivocally verified the hexagonal phase presence within the CuS particles. Notably, the investigation also unveiled a slightly sulfur-rich CuS NPs variant with an estimated bandgap energy of 3.8eV. Remarkably, this energy surpasses that of bulk CuS (1.85 eV), indicating a significant miniaturisation effect. The synthesized CuS NPs exhibited outstanding photocatalytic activity in the degradation of methyl Red (MR), showcasing remarkable efficiency under visible light irradiation. Sample S4 shows the best photocatalytic activity. This performance can be attributed to the presence of surface-bound OH ions on the CuS nanostructures, which facilitate the adsorption and acceleration of the degradation process for MR molecules. The catalyst managed to degrade 96.3% of the methyl red dye within just 190 minutes using a 0.2 g quantity, with higher sulphur ratio CuS nanostructures demonstrating the highest efficacy in achieving this remarkable degradation efficiency. Thus, our result is better than that reported by many research groups on the photocatalytic activity of CuS nanoparticles on dyes such as MB (Methylene Blue), CR (Congo Red), and RhB (Rhodamine B) [27-29], with percentage degradation ranging from 50 to 94.

REFERENCES

[1] Alivisatos, A. P., “Semiconductor Clusters, Nanocrystals and Quantum Dots”. Science, 1996, 271(5251), 933–937.

[2] Gahlaut, U. P. S., Kumar, V., Pandey, R. K., Goswami, Y. C. “Highly Luminescent Ultra Small Cu Doped ZnO Nanostructures Grown by Ultrasonicated Sol–Gel Route”. Optik 2016, 127(10), 4292–4295.

[3] Kshirsagar, U. A., Joshi, D. C., “Advancement in Fabrication of Sensors Using Nanotechnology: A Bibliographic Review and Future Research Scope”. Adv. Nano Res. 2023, 14(5), 399–407.

[4] Kumar, N., Purohit, L. P., Goswami, Y. C.,

"Spin Coating of ZnS Nanostructures on Filter Paper and Their Characterization". Phys. E: Low-Dimens. Syst. Nanostruct. 2016, 83, 333–338.

[5] Zhao, L., Zhou, L., Sun, C., Gu, Y., Wen, W., Fang, X., "Rose-Like CuS Microflowers and Their Enhanced Visible-Light Photocatalytic Performance". Cryst Eng Comm 2018, 20, 6529–6537.

[6] Riyaz, S., Parveen, A., Azam, A., "Microstructural and Optical Properties of CuS Nanoparticles Prepared by Sol-Gel Route". Perspect. Sci. 2016, 8, 632–635.

[7] Ding, T. Y., Wang, M. S., Guo, S. P., Guo, G. C., Huang, J. S., "CuS Nanoflowers Prepared by a Polyol Route and Their Photocatalytic Property". Mater. Lett. 2008, 62(30), 4529–4531.

[8] Chen, Y. B., Chen, L., Wu, L. M., "Water-Induced Thermolytic Formation of Homogeneous Core-Shell CuS Microspheres and Their Shape Retention on Desulfurization". Cryst. Growth Des. 2008, 8 (8), 2736–2740.

[9] Shamraiz, U., Hussain, R. A., Badshah, A., "Fabrication and Applications of Copper Sulfide (CuS) Nanostructures". J. Solid State Chem. 2016, 238, 25–40.

[10] Han, Y., Wang, Y., Gao, W., Wang, Y., Jiao, L., Yuan, H., Liu, S., "Synthesis of Novel CuS with Hierarchical Structures and Its Application in Lithium-Ion Batteries". Powder Technol. 2011, 212 (1), 64–68.

[11] Noor ul Ain, Nasir, J. A., Khan, Z., Butler, I. S., Rehman, Z., "Copper Sulfide Nanostructures: Synthesis and Biological Applications". RSC Adv. 2022, 12, 7550.

[12] Basu, M., Sinha, A. K., Pradhan, M., Sarkar, S., Negishi, Y., Pal, T., "Synthesis and Characterization of a Bi-Oxide Nanoparticle ZnO/CuO by Thermal Decomposition of Oxalate Precursor Method". Int. J. Nano Dimens. 2010, 1 (1), 33–40.

[13] Wang, L., "Synthetic Methods of CuS Nanoparticles and Their Applications for Imaging and Cancer Therapy". RSC Adv. 2016, 6, 82596–82615.

[14] Ghane, M., Sadeghi, B., Jafari, A., Paknejhad, A., "Synthesis and Characterization of a Bi-Oxide Nanoparticle ZnO/CuO by Thermal Decomposition of Oxalate Precursor Method". Int. J. Nano Dimens. 2010, 1 (1), 33–40.

[15] Sadeghi, B., Ghammamy, S., Gholipour, Z., Ghorchibeigy, M., Amini Nia, A., "Gold/Hydroxypropyl Cellulose Hybrid Nanocomposite Constructed with More Complete Coverage of Gold Nano-Shell". Micro Nano Lett. 2011, 6, 209–213.

[16] He, W., Jia, H., Li, X., Lei, Y., Li, J., Zhao, H., Mi, L., Zhang, L., Zheng, Z., "Understanding the Formation of CuS Concave Superstructures with Peroxidase-Like Activity". Nanoscale 2012, 4, 3501–3506.

[17] Kaundal, J. B., Goswami, Y. C., Sharma, R., "Optically Important Transparent Syndiotactic Polystyrene/FeS Composites Grown by Low Sol-Gel Route". Orient. J. Chem. 2022, 38 (3), 766–770.

[18] Cheng, Z., Wang, S., Wang, Q., Geng, B., "A Facile Solution Chemical Route to Self-Assembly of CuS Ball-Flowers and Their Application as an Efficient Photocatalyst". CrystEngComm 2010, 12, 144–149.

[19] Murugan, S., Garg, S., Singh, I., Rajendran, R., Santhosh, C., Chevva, H., Vanchinathan, T., Marepally, B., Grace, A., "Solvothermal Preparation of ZnO/Graphene Nanocomposites and Its Photocatalytic Properties". Nanoscience Nanotechnol. Lett. 2013, 5, 349–354.

[20] Roy, P., Srivastava, S. K., "Solvothermal Growth of Flowerlike Morphology from Nanorods of Copper Sulfides". J. Nanoscience Nanotech. 2008, 8 (3), 1523–1527.

[21] Palanisamy, S., Velmurugan, S., Yang, T. C. K., "One-Pot Sonochemical Synthesis of CuS Nanoplates Decorated Partially Reduced Graphene Oxide for Biosensing of Dopamine Neurotransmitter". Ultrason. Sonochem. 2020, 64, 105043.

[22] Kumar, N., Pathak, T. K., Purohit, L. P., Swart, H. C., Goswami, Y. C., "Self-Assembled Cu Doped CdS Nanostructures on Flexible Cellulose Acetate Substrates Using Low-Cost Sol–Gel Route". Nano-Structures Nano-Objects 2018, 16, 1–8.

[23] Mezgebe, M. M., Ju, A., Wei, G., Macharia, D. K., Guang, S., Xu, H., "Structure-Based Optical Properties and Catalytic Activities of Hydrothermally Prepared CuS Nanostructures". Nanotech

2019, 30 (1), 105704.
[24] Zhang, P., Gao, L., “Copper Sulfide Flakes and Nanodisks”. J. Mater. Chem. 2003, 13 (8), 2007–2010.
[25] Xu, H. L., Wang, W. Z., Zhu, W., “Sonochemical Synthesis of Crystalline CuS Nanoplates via an In Situ Template Route”. Mater. Lett. 2006, 60 (17–18), 2203–2206.
[26] Du, W., Qian, X., Xiaodong, M., Gong, Q., Cao, H., Yin, J., “Shape-Controlled Synthesis and Self-Assembly of Hexagonal Covellite (CuS) Nanoplatelets”. Chemistry 2007, 13 (11), 3241–3247.
[27] Ayodhya, D., Venkatesham, M., Kumari, A. S., Reddy, G. B., Ramakrishna, D., Veerabhadram, G., “Photocatalytic Degradation of Dye Pollutants under Solar, Visible, and UV Lights Using Green Synthesized CuS Nanoparticles”. J. Exp. Nanosci. 2016, 11, 418–432.
[28] Wu, H., Li, Y., Li, Q., “Facile Synthesis of CuS Nanostructured Flowers and Their Visible Light Photocatalytic Properties”. Appl. Phys. A 2017, 123, 196.
[29] Nancucheo, A., Segura, A., Hernandez, P., Hernandez-Montelongo, J., Pesenti, H., Arranz, A., Benito, N., Romero-Saez, M., Contreras, B., Díaz, V., et al. “Covellite Nanoparticles with High Photocatalytic Activity Bioproduced by Using H_2S Generated from a Sulfidogenic Bioreactor”. J. Environ. Chem. Eng. 2022, 10, 107409.
[30] Saranya, M., Grace, A. N., “Hydrothermal Synthesis of CuS Nanostructures with Different Morphology”. J. Nano Res. 2012, 18–19, 43–51.
[31] Umair, S., Hussain, A., Badshah, A., “Fabrication and Applications of Copper Sulfide (CuS) Nanostructures”. J. Solid State Chem. 2016, 238, 25–40.
[32] Savarimuthu, I., Susairaj, M. J. A. M., “CuS Nanoparticles Trigger Sulphite for Fast Degradation of Organic Dyes under Dark Conditions”. ACS Omega 2022, 7 (5), 4140–4149.
[33] Roy, P., Srivastava, S. K., “Nanostructured Copper Sulfides: Synthesis, Properties and Applications”. CrystEngComm 2015, 17, 7801–7815.
[34] Mote, V., Purushotham, Y., Dole, B., “Williamson-Hall Analysis in Estimation of Lattice Strain in Nanometer-Sized ZnO Particles”. J. Theor. Appl. Phys. 2012, 6, 6.
[35] Cullity, B. D., Stock, S. R., “Elements of X-Ray Diffraction”. 3rd ed.; Prentice-Hall Inc.: Upper Saddle River, NJ, 2001; pp 167–171.
[36] Riyaz, S., Parveen, A., Azam, A., “Microstructural and Optical Properties of CuS Nanoparticles Prepared by Sol-Gel Route”. Perspect. Sci. 2016, 8, 632–635.
[37] Koutu, V., Rajawat, S., Shastri, L., Malik, M. M., “Apoptosis and Inhibition of Human Epithelial Cancer Cells by ZnO Nanoparticles Synthesized Using Plant Extract”. Adv. Nano Res. 2019, 7 (4), 233–240.
[38] Kumar, N., Purohit, L. P., Goswami, Y. C., “Spin Coating of Highly Luminescent Cu Doped CdS Nanorods and Their Optical Structural Characterizations”. Chal. Lett. 2015, 12 (6), 333–338.
[39] Kumar, N., Purohit, L. P., Goswami, Y. C., “Synthesis of Cu Doped ZnS Nanostructures on Flexible Substrate Using Low-Cost Chemical Method”. AIP Conf. Proc. 2015, 1675 (1), 020030.
[40] Nagaich, S., Goswami, Y. C., “Shor’s Algorithm for Quantum Numbers Using MATLAB Simulator”. Proc. 5th Int. Conf. Adv. Comput. Commun. Technol. 2015, 5, 165–168.
[41] Zhu, S., Wang, D., “Photocatalysis: Basic Principles, Diverse Forms of Implementations and Emerging Scientific Opportunities”. Adv. Energy Mater. 2017, 7 (23), 1700841.
[42] Lv, M., Yang, L., Wang, X., Cheng, X., Song, Y., Yin, Y., Liu, H., Han, Y., Cao, K., Ma, W., Qi, G., Li, S., “Visible-Light Photocatalytic Capability and the Mechanism Investigation of a Novel PANI/Sn_3O_4 p–n Heterostructure”. RSC Adv. 2019, 9, 40694–40707.
[43] Ali, M. E., Alhathal, A. A., Azeez, F. A., Ghaly, M. Y., “Photoassisted Mineralization of Remazole Red F3B over NiO/TiO_2 and CdO/TiO_2 Nanoparticles under Simulated Sunlight”. Sep. Sci. Technol. 2018, 53, 170–180.